JOURNAL OF THE ROYAL SOCIETY Interface

High fidelity information processing in folic acid chemotaxis of *Dictyostelium* amoebae

Igor Segota, Surin Mong, Eitan Neidich, Archana Rachakonda, Catherine J. Lussenhop and Carl Franck

J. R. Soc. Interface 2013 **10**, 20130606, published 11 September 2013

JOURNAL OF THE ROYAL SOCIETY Interface

rsif.royalsocietypublishing.org

Research

Cite this article: Segota I, Mong S, Neidich E, Rachakonda A, Lussenhop CJ, Franck C. 2013 High fidelity information processing in folic acid chemotaxis of *Dictyostelium* amoebae. J R Soc Interface 10: 20130606.
http://dx.doi.org/10.1098/rsif.2013.0606

Received: 8 July 2013
Accepted: 22 August 2013

Subject Areas:
biophysics

Keywords:
chemotaxis, *Dictyostelium*, information theory

Author for correspondence:
Igor Segota
e-mail: is246@cornell.edu

Electronic supplementary material is available at http://dx.doi.org/10.1098/rsif.2013.0606 or via http://rsif.royalsocietypublishing.org.

Royal Society Publishing
Informing the science of the future

High fidelity information processing in folic acid chemotaxis of *Dictyostelium* amoebae

Igor Segota, Surin Mong, Eitan Neidich, Archana Rachakonda, Catherine J. Lussenhop and Carl Franck

Laboratory of Atomic and Solid State Physics, Cornell University, Ithaca, NY 14853, USA

Living cells depend upon the detection of chemical signals for their existence. Eukaryotic cells can sense a concentration difference as low as a few per cent across their bodies. This process was previously suggested to be limited by the receptor–ligand binding fluctuations. Here, we first determine the chemotaxis response of *Dictyostelium* cells to static folic acid gradients and show that they can significantly exceed this sensitivity, responding to gradients as shallow as 0.2% across the cell body. Second, using a previously developed information theory framework, we compare the total information gained about the gradient (based on the cell response) to its upper limit: the information gained at the receptor–ligand binding step. We find that the model originally applied to cAMP sensing fails as demonstrated by the violation of the data processing inequality, i.e. the total information exceeds the information at the receptor–ligand binding step. We propose an extended model with multiple known receptor types and with cells allowed to perform several independent measurements of receptor occupancy. This does not violate the data processing inequality and implies the receptor–ligand binding noise dominates both for low- and high-chemoattractant concentrations. We also speculate that the interplay between exploration and exploitation is used as a strategy for accurate sensing of otherwise unmeasurable levels of a chemoattractant.

1. Introduction

Eukaryotic amoebae *Dictyostelium discoideum* (referred as *Dictyostelium*) in the vegetative state forage on bacteria by following gradients of folic acid (FA), a by-product of bacterial metabolism [1,2]. It is currently believed that *Dictyostelium* measure chemical gradients directly by monitoring the distribution of the occupied chemoattractant receptors. These cells can detect concentration differences as low as a few per cent across their cell bodies [3–8] and it is currently an open question what exactly limits this process. Previously, the receptor–ligand binding fluctuations were suggested as the limiting factor, which remains a possibility because a single excited receptor may amplify the signal by activating multiple G-proteins [9–11].

The chemotaxis signalling system can be described as the following Shannon communication channel [12,13]: the chemoattractant gradient direction as the input, the spatial distribution of occupied receptors as the intermediate step and the direction of cell motion as the output. Fuller *et al*. [4] recently exploited this information-theoretic framework, where a cell in a static gradient was modelled as N receptors arranged in a circle, each in chemical equilibrium with the local chemoattractant concentration, described by a dissociation constant K_d.

The joint state of all receptors θ_{rec} was assumed to depend only on the gradient direction, θ_{grad}. Likewise, the probability of a cell moving in a direction θ_{res} was assumed to depend only on θ_{rec}, with these three variables forming a Markov chain: $\Theta_{grad} \rightarrow \Theta_{rec} \rightarrow \Theta_{res}$ (see the electronic supplementary material). Capital greek letters denote random variables and lowercase greek letters their values. Fuller *et al*. [4] computed the mutual information between the gradient

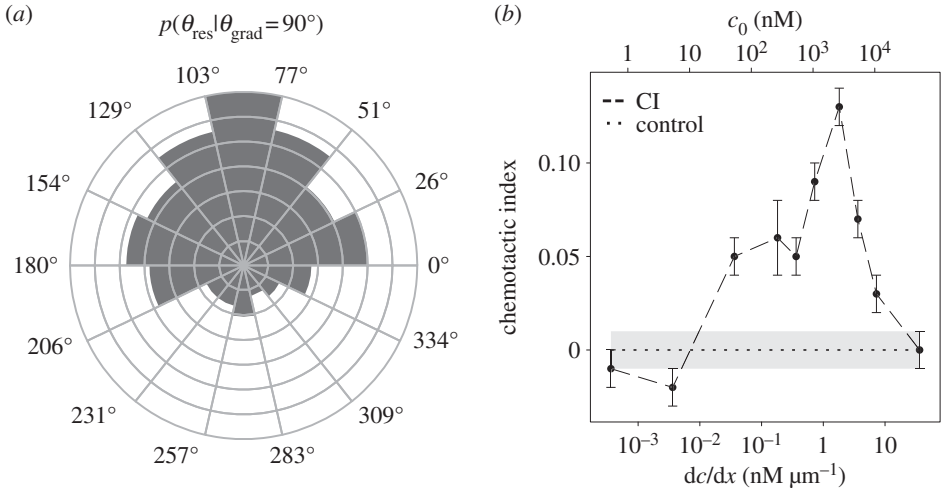

Figure 1. Measured chemotaxis response for a range of gradients and mean concentrations. (*a*) Distribution of cell displacement angles for the peak response for the gradient $dc/dx = 1.6$ nM μm^{-1} and mean concentration $c_0 = 2500$ nM. Each radial step represents 15 data points. (*b*) CI for experiments with variable FA concentration in the top channel, which changed both the mean concentration and the gradient. The controls denote CI for experiments performed with no gradient with mean FA concentrations of 0, 2500 and 10 000 nM. The error bars and grey area denote standard error of the mean (s.e.m.).

direction and the receptor distribution $I_{ext}(\Theta_{grad},\Theta_{rec})$, 'external mutual information'. I_{ext} quantifies the information gained about the gradient through a perfect (noiseless) readout of the occupied receptors.

Furthermore, Fuller *et al*. [4] used *Dictyostelium* cAMP chemotaxis experiments to calculate the mutual information between the gradient direction and the cell response $I_{tot}(\Theta_{grad}, \Theta_{res})$, 'total mutual information'. I_{tot} quantifies the information gained about the gradient by cells through the imperfect (noisy) readout of the occupied receptors. The data processing inequality [14, p. 34] states that in a Markov chain of variables, information can only be destroyed in each subsequent step, which here translates into $I_{tot} \leq I_{ext}$. In other words, the information gained by cells after being processed through the entire signalling pathway, cannot exceed the information gained at the receptor level. Fuller *et al*. [4] then argued that for low cAMP concentrations the receptor–ligand binding fluctuations dominate the entire noise ($I_{tot} \approx I_{ext}$), because there is no further information loss downstream. Previously, Ueda & Shibata [11] also reached this conclusion using signal-to-noise ratio arguments, using stochastic receptor noise and time integration with second messengers and locomotion systems.

Here, we measure the response of a population of *Dictyostelium* cells to static linear FA gradients, established in an agarose gel-based microfluidic device [15]. The steady-state gradients were achieved by maintaining fixed concentrations of FA on opposite sides of a microfluidic channel (see the electronic supplementary material). A linear gradient was established by diffusion through agarose gel. Cell migration was recorded using time-lapse optical microscopy. The measured distribution of cell displacement angles $p(\theta_{res}|\theta_{grad})$ was used to calculate the total mutual information I_{tot} and compared to I_{ext} (using the result in [4]) to test the possibility of receptor–ligand binding fluctuations dominating the total noise.

2. Results and discussion

First, we use the result in Fuller *et al*. ([4]; electronic supplementary material, equation S56) for the external mutual information I_{ext} for shallow linear gradients

$$I_{ext}(\Theta_{grad}, \Theta_{rec}) = \frac{N}{4 \ln 2\, c(x)} \left(\frac{\nabla c}{1 + c(x)} \right)^2, \qquad (2.1)$$

where $c(x)$ is the concentration measured in units of K_d, ∇c is the gradient measured in units of $K_d\, R^{-1}$ (R is the radius of a hemispherical cell, taken as 5 μm) and the dimensionless small parameter $\epsilon \equiv \nabla c/(1 + c) \ll 1$. For larger values of ϵ, one has to resort to numerical simulations. The design of our microfluidic device ensured it was applicable to use the equation (2.1) as the small parameter was in range $0.0003 \leq \epsilon \leq 0.0065$.

Previously, Wurster & Butz [16] and de Wit & van Haastert [17] measured the dissociation constants K_d and receptor numbers N using radioligand assays. Following Wurster & Butz [16], we used the measured N and K_d after 3 h in the buffer, which reflects the conditions in our experiments. As will be discussed below, following De Wit & van Haastert [17], we later considered multiple receptor types for which the only information available was for vegetative cells. Wurster & Butz [16] found $K_d = 150$ nM, $N = 60\,000$ and de Wit & van Haastert [17] found five receptor types with the following dissociation constants and receptor numbers: (i) $K_{d_1} = 450$ nM, $N_1 = 80\,000$, (ii) $K_{d_2} = 70$ nM, $N_2 = 80\,000$, (iii) $K_{d_3} = 17$ nM, $N_3 = 550$, (iv) $K_{d_4} = 50$ nM, $N_4 = 50$ and (v) $K_{d_5} = 15$ nM, $N_5 = 1450$. In both cases, Scatchard plots show that the first-order kinetics can be used with good approximation but that there is slight curvature implying either negative cooperativity or greater receptor heterogeneity. Furthermore, the binding curves for FA were measured for up to micromolar concentrations, the interesting range explored in this study.

Second, we measured the cell trajectories and the distribution of angles $p(\theta_{res}|\theta_{grad})$ of total displacement vectors (figure 1*a*) of a population of *Dictyostelium* cells (see the electronic supplementary material for Methods). In each experiment, the FA gradient was uniform and the concentration varied at most three-fold across the width of a channel. Each experiment was repeated until we obtained 300–700 cell trajectories. These observations were used to calculate the total mutual information I_{tot} and the chemotactic index (CI). CI is defined as $\mathrm{CI} = \left(\sum_i \boldsymbol{r}_i\right) \cdot \hat{n} / \sum_i |\boldsymbol{r}_i|$, where $\boldsymbol{r}_i$

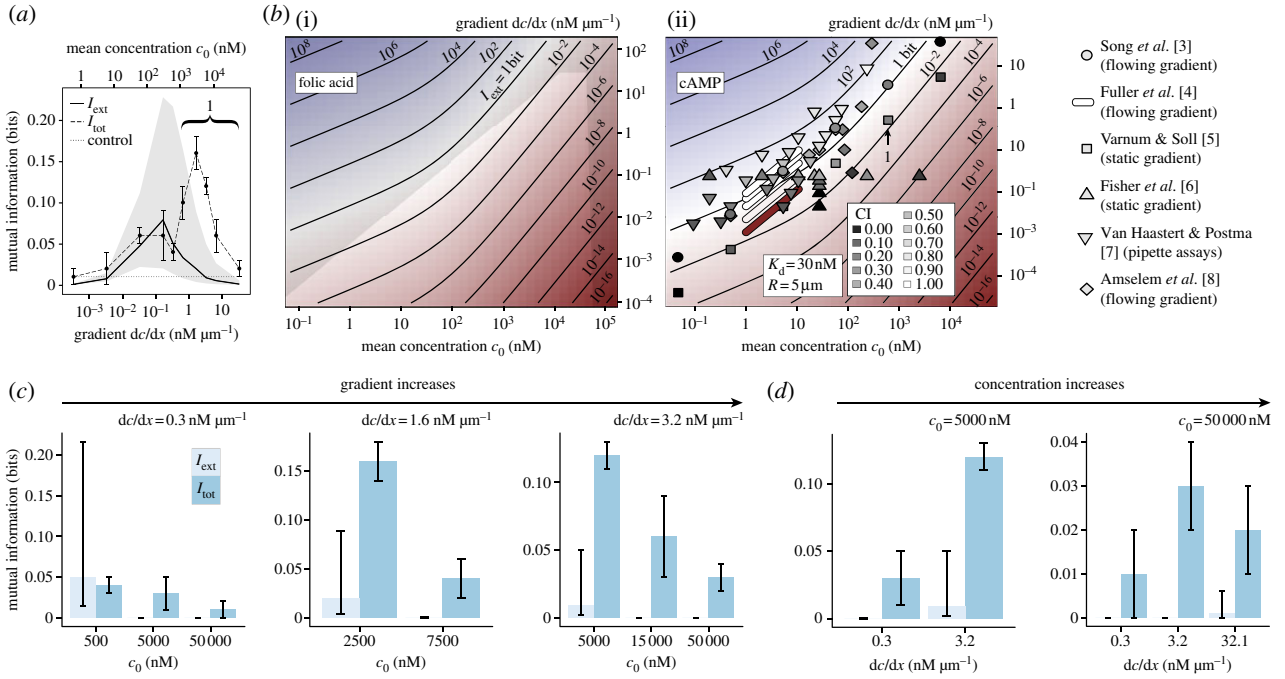

Figure 2. Comparison of the total mutual information I_{tot} and external mutual information I_{ext}. (*a*) I_{tot} (dashed line) and I_{ext} (solid line) for the same experiments as in figure 1*a*, both averaged over all local concentrations (see the electronic supplementary material). Error bars for I_{tot} represent s.e.m. The shaded range for I_{ext} denotes its spread owing to the range of local concentrations the cells were exposed to in the microfluidic device (see text). Dotted line denotes the I_{tot} for control experiments without a gradient. Annotation 1 shows the range where the data processing inequality is strongly violated, $I_{tot} > I_{ext}$. (*b*) (i) Calculated values for I_{ext} (equation (2.1)); shaded area denotes the combinations of c_0 and dc/dx inaccessible in our experiment owing to the geometry of the microfluidic device and low solubility of FA in development buffer (approx. 0.1 mM). (ii) the range of concentrations and gradients where cAMP chemotaxis has been measured, coloured by the value of measured CI. The measurement with annotation 1 ($c_0 = 500$ nM $= 17\ K_d$, dc/d$x = 0.5$ nM μm$^{-1} = 0.08\ K_d\ R^{-1}$, CI $= 0.25$) is done in the approximate range where we detected the greatest violation of the data processing inequality ($c_0 = 5000$ nM $= 33\ K_d$, dc/d$x = 3.2$ nM μm$^{-1} = 0.11\ K_d/R$, CI $= 0.13$, $I_{tot} = 0.16$ bits) if we compare them by rescaling the concentrations with their respective K_ds (K_d(cAMP) = 30 nM, K_d(FA) = 150 nM [16,18]). I_{tot} and I_{ext} for experiments with fixed gradient, where mean concentration changed is shown in (*c*) and experiments with fixed mean concentration where the gradient is changed are shown in (*d*). In the range investigated here, increasing the concentration and reducing the gradient reduced the chemotaxis response, I_{tot} but the violation of the data processing inequality persists. (Online version in colour.)

the instantaneous cell displacement during the time step i (taken as 30 s) and $\hat{n}$ is the gradient direction.

We performed 10 experiments where we varied the FA concentration in the top channel of a microfluidic device while keeping the bottom channel at concentration zero. In these experiments, both the concentration and the gradient were changed and these are plotted in figure 2*a*. We also performed five additional experiments (shown in figure 2*c*,*d*) where we changed the mean concentration and the gradient separately. For the range of concentrations and gradients explored here, decreasing the gradient and increasing FA concentration diminished the signal. Therefore, the FA chemotaxis can depend both on the absolute value of FA concentration and its gradient.

I_{tot} was calculated by segmenting the real interval $0 \leq \theta_{res} < 2\pi$ into m bins of equal width. The bin size was $m = 14$ for all experiments, because I_{tot} with that bin size correlated extremely well with CI (compare figures 1*b* and 2*a*) for which no binning was used (see the electronic supplementary material for further analysis). The fraction of total displacement angles n_j ending up in the bin $\theta_{res,j} \leq \theta < \theta_{res,j+1}$ was counted and I_{tot} was computed [14, pp. 247–248] as

$$I_{tot}(\Theta_{grad}, \Theta_{res}) = \sum_{j=1}^{m} n_j \log n_j + \log m, \qquad (2.2)$$

with the error due to a finite number of data points estimated as $(m-1)/2M$ [19], where M is the total number of data points.

Next, we compared I_{tot} and I_{ext}. Figure 2*a* shows that for low concentrations and shallow gradients $I_{tot} \approx I_{ext}$, meaning the receptor–ligand binding fluctuations dominate the total noise. This possibility was previously suggested for cAMP [7,11] using signal-to-noise ratio analysis with a biased random walk model of cell motion. The information-theoretic analysis assumes only the steady-state receptor–ligand binding fluctuations and benefits from not being tied to a particular model of cell motion, because *Dictyostelium* cells do not follow a simple random walk [20].

The most surprising result is that the response is observed for gradients as low as 0.2% across the cell body (dc/d$x = 3.2$ nM μm^{-1}, $c_0 = 15\,000$ nM, $I_{tot} = 0.06$ bits shown in figure 2*b*). For these experiments, the difference in the fraction of occupied receptors front-to-back on the cell body is given by

$$\eta = \frac{c_{front}}{c_{front} + K_d} - \frac{c_{back}}{c_{back} + K_d} \qquad (2.3)$$

and is shown in table 1 for different measured dissociation constants. This fraction is at most 0.006% which amounts to a 1–10 receptors difference with 29 700 receptors (or 99%) occupied on each side, indicating a highly saturated regime. Furthermore, in this range, the data processing inequality ($I_{tot} \leq I_{ext}$) is strongly violated as we have $I_{tot} > I_{ext}$, with high certainty. The observed response is better than theoretically possible with receptor–ligand binding fluctuations as the only noise source. Next, we compared our results with previous cAMP chemotaxis experiments [3–8], shown in figure 2*b*. In comparing critical parameters, the receptor–ligand binding constant K_d(FA) = 150 nM stands out as a factor of five greater

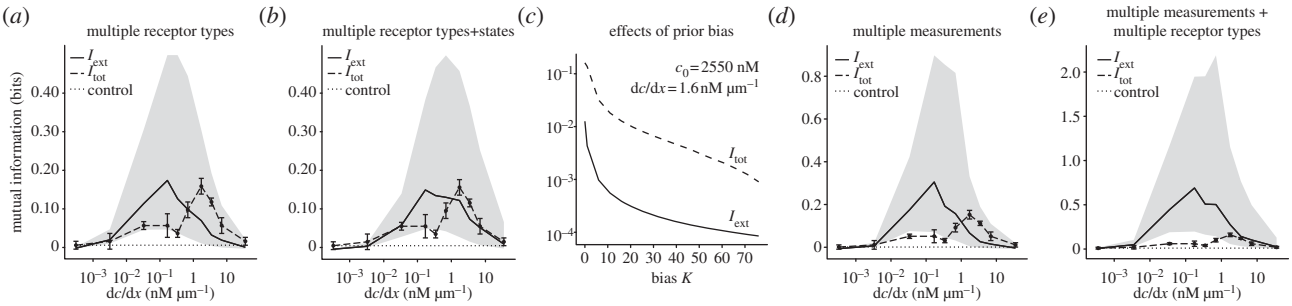

Figure 3. I_{tot} and I_{ext} for models with additional assumptions. (*a*) Fit of our data to the model with multiple receptor types; see text for details. (*b*) Fit of our data to the model with multiple receptor types and the hypothesis that they can be phosphorylated to states with three-fold higher K_d= 1350 nM. (*c*) Calculation for biased I_{tot} and I_{ext}, where the uniform prior distribution was replaced with a circular normal distribution. Both I_{tot} and I_{ext} are plotted as a function of bias parameter K (large K values correspond to very sharp prior distributions), showing that the violation of data processing inequality persists even for biased cells. (*d*) Comparison of I_{tot} and I_{ext} for a model with multiple independent measurements of receptor occupancy which still results in the violation of the data processing inequality. (*e*) Model with combined effects of (*a*) and (*d*) does not result in the violation of the data processing inequality and successfully explains the data.

Table 1. Fraction of occupied receptors front to back of the cell for the shallowest gradient where we measured the chemotaxis response, calculated using each measured receptor type according to equation (2.3).

K_d (nM)	450	150	70	50	17	15
η (%)	0.006	0.002	0.001	0.0007	0.0002	0.0002

compared with cAMP, K_d(cAMP) = 30 nM, whereas the number of receptors per cell is almost the same: 60 000 for FA and 70 000 for cAMP [16,18].

These simplified descriptions of FA and cAMP receptors were sufficient to explain the results in Fuller *et al*. [4], but do not suffice here—possibly explained by the limited range of cAMP concentrations and gradients investigated in [4] (figure 2*b*). The measurement with annotation 1 on fig. 2b from Varnum & Soll [5] supports this possibility. They measured CI = 0.25 for cAMP, compared to our CI = 0.13 for FA, for roughly the same mean concentration c_0 and gradient dc/dx. Therefore, the cAMP response in that range might also result in the violation of the data processing inequality. Motivated by the failure of the theory, we investigated five different modifications of the original model.

2.1. Effects of folic acid deaminase

First, we considered reduced FA concentrations perceived by cells as a result of FA deaminase activity, a protein that degrades FA [21]. We concluded, using both calculation and a series of control experiments (see the electronic supplementary material), that it does not significantly contribute to the observed result.

2.2. Effects of multiple receptor types and receptor phosphorylation

Second, we considered all different receptor types mentioned previously. This possibility was motivated by the local minimum in I_{tot} shown in figure 2*a* indicating that perhaps there are two receptor types or states, each active in a distinct range of local ligand concentrations. We calculated I_{ext} for each receptor type and added them together to investigate whether this resolves the violation of the data processing inequality. The results are shown in figure 3*a* and indicate that the presence of multiple receptor types reduces but does not eliminate the violation of the data processing inequality. This is because the shaded range for I_{ext} in figure 3 represents the range of concentrations the cells were exposed to in our microfluidic device (and not the uncertainty), with the maximum value of I_{ext} corresponding to the bottom of our device and the minimum value corresponding to the top of our device. However, the systematic uncertainty of the average I_{ext} (solid line in figure 3*a*) is only 10% (see the electronic supplementary material), which is what is compared to the average I_{tot} (we appreciate the comments of anonymous referees and Eric Siggia on this matter.) Furthermore, the double-peak feature observed in I_{tot} is not exactly reproduced in I_{ext} even when considering only two receptor types. This could be owing to the fact that I_{ext} is only an upper limit for I_{tot}, and in this range, the intracellular signal processing is not negligible, so $I_{tot} \ll I_{ext}$. In other words, the dip could be the consequence of the extra noise somewhere downstream of the receptor–ligand binding events. It is also worth mentioning that this double-peak response prevents us from using any single receptor with fixed K_d to fix the violation of the data processing inequality, unless the receptor number per cell N is set to a factor 12 more than it is measured.

Therefore, this explanation could be plausible only if all the cells were concentrated near the bottom of our device. In our experiments, they were always uniformly distributed with the mean position in the centre.

Third, we hypothesized that FA receptors can be phosphorylated. Xiao *et al*. [22] have shown that the phosphorylation of cAMP receptors cAR1 reduced the affinity (increased K_d) of a cAMP–cAR1 process by a factor of three, from 300 to 900 nM. Here, we assume that the additional receptor types can be phosphorylated to $3 \times K_d$ and fit the data in the same way as for additional receptor types. The results (figure 3*b*) show that this only reduced the violation of the data processing inequality, but did not eliminate it.

2.3. Effects of cell polarization

Fourth, we considered for the possibility of cell polarization (we thank an anonymous referee for this suggestion),

previously considered in Andrews & Iglesias [13] and Hu *et al*. [23]. In our analysis thus far, we assumed that cells had no previous knowledge of the gradient direction, so the prior probability was $p(\theta_{\mathrm{grad}}) = 1/2\pi$. Now, we consider a circular normal prior distribution

$$p(\theta_{\mathrm{grad}}) = \frac{\exp(K\cos\theta_{\mathrm{grad}})}{2\pi I_0(K)}, \tag{2.4}$$

where $I_0(K)$ is the modified Bessel function of the first kind of zeroth order, and the parameter K measures the bias strength. We used the approach from Hu *et al*. [23] to numerically calculate $I_{\mathrm{ext}}^{\mathrm{bias}}(K)$. We also numerically calculated $I_{\mathrm{tot}}^{\mathrm{bias}}(K)$ (see the electronic supplementary material) and then compared both $I_{\mathrm{tot}}^{\mathrm{bias}}$ and $I_{\mathrm{ext}}^{\mathrm{bias}}$ up to very biased distributions with $K = 80$, as larger values required significantly higher numerical precision. Figure 3*c* shows that the violation of the data processing inequality still persists.

2.4. Effects of multiple measurements

Finally, we investigated the effect of multiple independent measurements of the receptor occupancy [7,11], occurring if cells can choose between (i) short and imprecise gradient measurements but moving fast, and (ii) long and precise gradient measurements but moving more slowly. This is known as the trade-off between exploration and exploitation in the field of reinforcement learning [24].

Equation (2.1) is only valid for a single snapshot measurement. The information acquired from multiple independent measurements is simply the sum of the information of each contribution owing to a single measurement. Therefore, we multiply the equation (2.1) by the number of independent measurements $N_{\mathrm{meas}} = T_{\mathrm{pseudo}}/T_{\mathrm{correl}}$ [4,23], where T_{pseudo} is the time scale of pseudopod extension and T_{correl} is the receptor correlation time (this ratio gives us the maximum number of measurements that could have been performed). We note that T_{pseudo} is likely the upper bound for the integration time based on the evidence in variable gradient experiments [25] where it was observed that the cells extend their pseudopods in the gradient direction as soon as the direction of the gradient is changed. Rappel & Levine [26,27] previously noted that the correlation time depends on both receptor chemical dynamics and the diffusive process. They estimated the cAMP receptor correlation time $T_{\mathrm{correl}} = 5$ s. Fuller *et al*. [4] concluded $N_{\mathrm{meas}}^{\mathrm{cAMP}} \approx 1$. Accordingly, we estimated $N_{\mathrm{meas}}^{\mathrm{FA}}$ by assuming that T_{pseudo} is inversely proportional to the mean cell speed, and the same T_{correl} for both FA and cAMP receptors (based on comparable receptor off-rates for FA and cAMP receptors [17,28])

$$N_{\mathrm{meas}}^{\mathrm{FA}} = \frac{T_{\mathrm{pseudo}}^{\mathrm{FA}}}{T_{\mathrm{correl}}} \approx N_{\mathrm{meas}}^{\mathrm{cAMP}} \frac{v_{\mathrm{cAMP}}}{v_{\mathrm{FA}}}, \tag{5}$$

where the chemotaxis speeds are $v_{\mathrm{cAMP}} = 0.25\ \mu\mathrm{m\,s^{-1}}$ [4] and $0.05\ \mu\mathrm{m\,s^{-1}} \le v_{\mathrm{FA}} \le 0.12\ \mu\mathrm{m\,s^{-1}}$, which gives $2 \le N_{\mathrm{meas}}^{\mathrm{FA}} \le 4$. I_{tot} and I_{ext} are compared in figure 3*d* and show that this only reduced the violation of the data processing inequality, but again does not eliminate it. Recently developed approaches considered diffusible inhibitors in balanced inactivation model [26,27,29] and their integration time ($T_{\mathrm{int}} = 10$ s) corresponds roughly to the integration times estimated here ($T_{\mathrm{int}} = 10$–20 s). In addition, the models considered so far do not reproduce the double peak observed experimentally (figure 3), but this might be the consequence of a significant information loss downstream of the receptor–ligand binding events.

However, combining the effects of additional receptor types and multiple independent measurements does not result in the violation of the data processing inequality (figure 3*e*). $N_{\mathrm{meas}}^{\mathrm{FA}}$ roughly agrees with [7] $N_{\mathrm{meas}}^{\mathrm{cAMP}} \approx 2$, which was included to explain a much greater range of concentrations and gradients than in [4] (figure 2*b*).

It should still be noted that the multiple independent measurements can be a consequence of integrating the information from multiple pseudopods (we thank an anonymous referee for this suggestion). During the 30 s time interval, cells extend a number of small protrusions (sometimes simultaneously), some of which are retracted quickly (see fig. 6 in [30]). Taking this into account would lead to a different definition of the total mutual information than that used here where the centroid of each cell is used to specify its position. One direction for future studies is then to perform experiments with higher resolution to quantify the information acquired about the gradient using this alternative measure.

2.5. Other effects

Figure 3*e* implies that the total noise is indeed dominated by the receptor–ligand binding fluctuations at both low and high gradients and concentrations. This seems plausible because in that range, the receptors are either mostly unoccupied or occupied. In the intermediate range where $I_{\mathrm{ext}} \gg I_{\mathrm{tot}}$, the internal noise dominates. We note that it has been shown [31] that there is always a fraction of cell population which does not respond to gradients and polarizes in random directions, independent of the external cAMP gradient. Since in our experiments we only have static gradients, we could not separately identify these cells and they had to be included in the data analysis. Exclusion of this subpopulation from our analysis would increase the total mutual information I_{tot} even further and the violation of the data processing inequality would be even larger.

The possibility of receptor interactions was ruled out owing to uniform receptor distributions for both FA [32] and cAMP receptors [33,34]. Unlike in the cAMP case [4], here the non-circularity of cell shapes is not an issue because the cells are circular when sensing FA. However, there is still a possibility of a more complicated mechanism if FA receptors also transport FA into the cell [9], serving as a different communication channel, or if a FA transporter is a separate protein, as a separate communication channel.

The possibility that FA and cAMP receptors share the majority of the internal signalling pathway [35] implies equal FA and cAMP responses, if rescaled by their respective parameters K_{d} and N. This remains to be investigated with more cAMP and FA chemotaxis measurements in the same concentration and gradient range. The results here and in [4,11] confirmed that the external noise dominates for both chemoattractants in low concentration range. This is in contrast to the conclusion reached in the Supplementary Information of Samadani & Mettetal [31], SI possibly caused by using single-pulse temporal gradients, as opposed to defined static gradients used here and in [4].

Acknowledgements. We thank Petra Fey (Dicty Stock Center, Northwestern University) for AX4 cell lines, advice and suggestions about media preparation, Richard Kessin (Columbia University), Jeffrey Hadwiger (Oklahoma State University), David Knecht (University of Connecticut) for valuable advice regarding the

choice and preparation of chemotacting media and helpful suggestions, Elijah Bogart (Cornell University) for contributions to the microfluidic device design and strategic planning, Mingming Wu (Cornell University), Kevin Tharratt (Cornell University) for fruitful discussions, Kees Weijer (University of Dundee), Ariana Strandburg-Peshkin (Princeton University), Eric Siggia (Rockefeller University/Cornell University) and Nives Skunca (ETH Zurich) for useful comments, Herbert Levine and Wouter-Jan Rappel (University of California, San Diego) for helpful advice, Eberhard Bodenschatz (Max Planck Institute Goettingen, Germany/Cornell University) for generous advice and equipment, anonymous referees for helpful and insightful suggestions and ACCEL Cornell Engineering Lab for use of the COMSOL Multiphysics software.

Funding statement. This work was supported by National Institutes of Health grant (P01 GM078586).

References

1. Kessin RH. 2001 *Dictyostelium: evolution, cell biology, and the development of multicellularity*. Cambridge, UK: Cambridge University Press.
2. Pan P, Hall EM, Bonner JT. 1972 Folic acid as second chemotactic substance in the cellular slime moulds. *Nat. New Biol.* **237**, 181–182. (doi:10.1038/newbio237181a0)
3. Song L, Nadkarni SM, Bodeker HU, Beta C, Bae A, Franck C, Rappel W-J, Loomis WF, Bodenschatz E. 2006 *Dictyostelium discoideum* chemotaxis: threshold for directed motion. *Eur. J. Cell Biol.* **85**, 981–989. (doi:10.1016/j.ejcb.2006.01.012)
4. Fuller D, Chen W, Adler M, Groisman A, Levine H, Rappel W-J, Loomis WF. 2010 External and internal constraints on eukaryotic chemotaxis. *Proc. Natl Acad. Sci. USA* **107**, 9656–9659. (doi:10.1073/pnas.0911178107)
5. Varnum B, Soll DR. 1948 Effects of cAMP on single cell motility in *Dictyostelium*. *J. Cell Biol.* **99**, 1151–1155. (doi:10.1083/jcb.99.3.1151)
6. Fisher PR, Merkl R, Gerisch G. 1989 Quantitative analysis of cell motility and chemotaxis in *Dictyostelium discoideum* by using an image processing system and a novel chemotaxis chamber providing stationary chemical gradients. *J. Cell Biol.* **108**, 973–984. (doi:10.1083/jcb.108.3.973)
7. van Haastert PJM, Postma M. 2007 Biased random walk by stochastic fluctuations of chemoattractant–receptor interactions at the lower limit of detection. *Biophys. J.* **93**, 1787–1796. (doi:10.1529/biophysj.107.104356)
8. Amselem G, Theves M, Bae A, Beta C, Bodenschatz E. 2012 Control parameter description of eukaryotic chemotaxis. *Phys. Rev. Lett.* **109**, 108103. (doi:10.1103/PhysRevLett.109.108103)
9. Lauffenburger DA, Linderman JJ. 1993 *Receptors: models for binding, trafficking and signaling*, p. 335. Oxford, UK: Oxford University Press.
10. Devreotes PN, Zigmond SH. 1988 Chemotaxis in eukaryotic cells: a focus on leukocytes and *Dictyostelium*. *Annu. Rev. Cell Biol.* **4**, 649–686. (doi:10.1146/annurev.cb.04.110188.003245)
11. Ueda M, Shibata T. 2007 Stochastic signal processing and transduction in chemotactic response of eukaryotic cells. *Biophys. J.* **93**, 11–20. (doi:10.1529/biophysj.106.100263)
12. Shannon CE. 1948 A mathematical theory of communication. *Bell Syst. Tech. J.* **27**, 379–423 & 623–656. (doi:10.1002/j.1538-7305.1948.tb01338.x)
13. Andrews BW, Iglesias PA. 2007 An information-theoretic characterization of the optimal gradient sensing response of cells. *PLoS Comput. Biol.* **3**, e153. (doi:10.1371/journal.pcbi.0030153)
14. Cover TM, Thomas JA. 2005 *Elements of information theory*, 2nd edn, pp. 34–35. New York, NY: Wiley.
15. Cheng SY, Heilman S, Wasserman M, Archer S, Shulerac ML, Wu M. 2007 A hydrogel-based microfluidic device for the studies of directed cell migration. *Lab Chip* **7**, 763–769. (doi:10.1039/b618463d)
16. Wurster B, Butz U. 1980 Reversible binding of the chemoattractant folic acid to cells of *Dictyostelium discoideum*. *Eur. J. Biochem.* **109**, 613–618. (doi:10.1111/j.1432-1033.1980.tb04834.x)
17. De Wit RJW, van Haastert PJM. 1985 Binding of folates to *Dictyostelium discoideum* cells. Demonstration of five classes of binding sites and their interconversion. *Biochim. Biophys. Acta* **814**, 199–213. (doi:10.1016/0005-2736(85)90438-9)
18. van Haastert PJM. 1983 Binding of cAMP and adenosine derivatives to *Dictyostelium discoideum* cells. *J. Biol. Chem.* **258**, 9643–9648.
19. Roulston MS. 1999 Estimating the errors on measured entropy and mutual information. *Physica D* **125**, 285–294. (doi:10.1016/S0167-2789(98)00269-3)
20. Li L, Norrelykke SF, Cox EC. 2008 Persistent cell motion in the absence of external signals: a search strategy for eukaryotic cells. *PLoS ONE* **3**, e2093. (doi:10.1371/journal.pone.0002093)
21. Kakebeeke PIJ, De Wit RJW, Konijn TM. 1980 Folic acid deaminase activity during development in *Dictyostelium discoideum*. *J. Bacteriol.* **143**, 307–312.
22. Xiao Z, Yao Y, Long Y, Devreotes P. 1999 Desensitization of G-protein coupled receptors: agonist-induced phosphorylation of the chemoattractant receptor cAR1 lowers its intrinsic affinity for cAMP. *J. Biol. Chem.* **274**, 1440–1448. (doi:10.1074/jbc.274.3.1440)
23. Hu B, Chen W, Levine H, Rappel WJ. 2011 Quantifying information transmission in eukaryotic gradient sensing and chemotactic response. *J. Stat. Phys.* **142**, 1167–1186. (doi:10.1007/s10955-011-0156-4)
24. Sutton RS, Barto AG. 1998 *Reinforcement learning: an introduction* (*adaptive computation and machine learning*). Cambridge, MA: MIT Press.
25. Srinivasan K, Wright GA, Hames N, Housman M, Roberts A, Aufderheide KJ, Janetopoulos C. 2013 Delineating the core regulatory elements crucial for directed cell migration by examining folic-acid-mediated responses. *J. Cell Sci.* **126**, 221–233. (doi:10.1242/jcs.113415)
26. Rappel WJ, Levine H. 2008 Receptor noise and directional sensing in eukaryotic chemotaxis. *Phys. Rev. Lett.* **100**, 228101. (doi:10.1103/PhysRevLett.100.228101)
27. Rappel WJ, Levine H. 2008 Receptor noise limitations on chemotactic sensing. *Proc. Natl Acad. Sci. USA* **105**, 19 270–19 275. (doi:10.1073/pnas.0804702105)
28. Ueda M, Sako Y, Tanaka T, Devreotes P, Yanagida T. 2001 Single molecule analysis of chemotactic signaling in *Dictyostelium* cells. *Science* **294**, 864–867. (doi:10.1126/science.1063951)
29. Levine H, Kessler DA, Rappel WJ. 2006 Directional sensing in eukaryotic chemotaxis: a balanced inactivation model. *Proc. Natl Acad. Sci. USA* **103**, 9761–9766. (doi:10.1073/pnas.0601302103)
30. Xiong Y, Kabacoff C, Franca-Koh J, Devreotes PN, Robinson DN, Iglesias PA. 2010 Automated characterization of cell shape changes during amoeboid motility by skeletonization. *BMC Syst. Biol.* **4**, 33. (doi:10.1186/1752-0509-4-33)
31. Samadani A, Mettetal J, van Oudenaarden A. 2006 Cellular asymmetry and individuality in directional sensing. *Proc. Natl Acad. Sci. USA* **103**, 1549–1554. (doi:10.1073/pnas.0601909103)
32. Rifkin JL. 2001 Folate reception by vegetative *Dictyostelium discoideum* amoebae: distribution of receptors and trafficking of ligand. *Cell Motil. Cytoskeleton* **48**, 121–129. (doi:10.1002/1097-0169(200102)48:2<121::AID-CM1003>3.0.CO;2-Z)
33. Xiao Z, Zhang N, Murphy DB, Devreotes PN. 1997 Dynamic distribution of chemoattractant receptors in living cells during chemotaxis and persistent stimulation. *J. Cell. Biol.* **139**, 365–374. (doi:10.1083/jcb.139.2.365)
34. Skoge M. 2009 Receptor–receptor interactions in gradient sensing. PhD thesis. See http://www.princeton.edu/physics/graduate-program/theses/theses-from-2009/M.Skogethesis.pdf.
35. King JS, Insall RH. 2009 Chemotaxis: finding the way forward with *Dictyostelium*. *Trends Cell Biol.* **19**, 523–530. (doi:10.1016/j.tcb.2009.07.004)

Surprisingly high fidelity information processing in folic acid chemotaxis of Dictyostelium amoebae: Supplementary Information

Igor Segota, Surin Mong, Eitan Neidich, Archana Rachakonda, Catherine J. Lussenhop and Carl Franck
Laboratory of Atomic and Solid State Physics, Cornell University, Ithaca, NY 14853 (USA)

METHODS

Information measures

Shannon's information theory frees the data analysis from being tied to any particular model (as an example of successful applications see e.g. [1] and [2]) – and in this case, from any particular details of signal transduction pathways, but still provides quantifiable relationships between inputs and outputs. The relevant quantities in information theory are defined as follows [3]. The information entropy of a random variable X, is measured in bits defined as $H(X) = -\int p(x)\log_2 p(x)dx$ (a definite integral defined over the entire range where X is defined). It is a measure of "sharpness" of probability distribution $p(x)$; a perfectly sharp probability distribution has entropy zero, whereas a perfectly flat, uniform distribution gives the highest possible value for entropy $H(X)$. An alternative interpretation of information entropy is the number of bits or the amount of information required to describe the random variable X. Sharp probability distributions require fewer bits for their full description than flat probability distributions. Intuitively, for the former only a few values near the peak can be sufficient to describe most of the outcomes of X, while for the latter we need more information to achieve the same. For conditional probability distributions, the conditional entropy is measured in bits defined as $H(X|Y) = -\int dyp(y)\int dxp(x|y)\log_2 p(x|y)$. This measures how sharp $p(x|y)$ is, when averaged over all possible values of y. For some values y, $p(x|y)$ may be sharp, for some other values of y, $p(x|y)$ may not be so sharp, and the conditional entropy tells us on average what is the sharpness, when averaged over all possible y. The average *gain* in information about x, given y, is the difference between the two, called mutual information $I(X,Y) = H(X) - H(X|Y)$. This measure describes the increase in knowledge about X after we have been given some value y, and then averaged over all possible y. In other words, $I(X,Y)$ describes how much on average $p(x|y)$ is sharper, when compared to $p(x)$. The sharper the probability distribution becomes, the more information we have acquired about a random variable X.

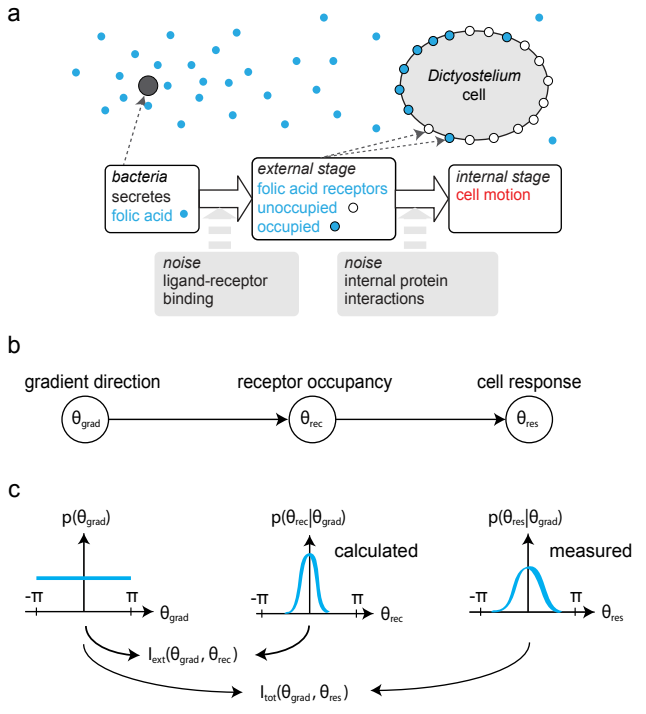

FIG. 1. The current paradigm for eukaryotic chemotaxis and the model assumptions. (a) Bacteria secrete folic acid (FA), which then binds to *Dictyostelium* FA receptors. *Dictyostelium* measures spatial distribution of occupied folic acid receptors and these binding events trigger a cascade of intracellular events eventually leading to cell movement. (b) Markov chain model assumption used in our work: the receptor occupancy θ_{rec} depends on the gradient θ_{grad}, and the cell response θ_{res} conditionally depends on the gradient. (c) The external (I_{ext}) and total mutual information (I_{tot}) compared in this work. As detailed in Methods, I_{ext} measures the information gained about the gradient, given the calculated spatial distribution of bound receptors, while I_{tot} measures the information gained given the distribution of cell responses. Assuming the Markov chain relationship in part b), the data processing inequality states $I_{tot} \leq I_{ext}$.

Application to gradient sensing

In this case, the sensing process essential to eukaryotic chemotaxis is depicted in Fig. 1a. Here we consider three random but conditionally dependent variables, the gradient direction θ_{grad}, the receptor occupancy θ_{rec} and the cell response directions θ_{res}. These variables are assumed to form a Markov chain (see Fig.1b), where the cell response is conditionally dependent on the distribution of occupied receptors; i.e. given the distribution of occupied receptors, the cell response is completely independent of the original direction of the gradient that caused this particular receptor occupancy. Due to noise, the same receptor occupancy distribution can occur for gradients pointing in different directions. Without any prior knowledge we assume the gradient is equally likely to be pointing in any direction. We will see how much information we can obtain about the gradient by either observing the cell response and by calculating the distribution of receptor occupancy, and then comparing the two gains. The mutual information $I_{tot}(\theta_{grad},\theta_{res}) = H(\theta_{grad}) - H(\theta_{grad}|\theta_{res})$ quantifies the total amount of information cells gained about the gradient (or by how much the entropy of θ_{grad} is reduced); this is determined by observing their response (see Fig.1c). Therefore, I_{tot} is the gain in information that includes all possible noise sources in the FA signal transduction

pathway.

In addition, the (external) mutual information (see Fig.1c) between the gradient direction and receptor occupancy $I_{ext}(\theta_{grad}, \theta_{rec}) = H(\theta_{grad}) - H(\theta_{grad}|\theta_{rec})$ tells us the information gained about the gradient by knowing the distribution of receptors occupied with FA. Authors in [4] formulated a theory for computing this quantity and gave an analytical result applicable for shallow gradients. The assumptions behind this theory are: i) the steady state of the receptor-ligand binding process, ii) the first part of the Markov chain model shown in Fig.1b (receptor probability distribution is affected only by the local gradient), iii) cells of perfectly circular shapes and iv) uniform receptor distribution. While we have no direct way of confirming the plausible assumptions i) and ii) when sensing FA, *Dictyostelium* do have circular shapes and the distribution of FA receptors was previously measured as uniform [5]. This theory gives predictions for the external mutual information I_{ext} using only two biochemical constants – the dissociation constant K_d between FA and its receptor and the total receptor number per cell, N. Both have been measured previously and multiple receptor types/states have been discovered as is also the case for cAMP receptors (see main text for discussion). The dissociation constant and the total receptor number per cell, as well as the experimentally fixed FA concentration and its gradient in our devices are sufficient to predict the external mutual information I_{ext}. I_{ext} provides the upper limit for the amount of information that can be acquired (I_{tot}), due to the data processing inequality: $I_{tot} \leq I_{ext}$ [7]. In other words, any kind of data processing can only destroy information. If the two quantities are roughly similar $I_{tot} \approx I_{ext}$, then the gain in information about θ_{grad} is about the same for both cases and the majority of the noise in the entire process comes from receptor-ligand binding events.

Cell growth and preparation

Cells of the well characterized axenic strain, AX4 (provided by Dictyostelium Stock Center, Northwestern University), were grown in shaken culture suspension at 150 RPM in Formedium HL5 (Formedium, Hunstanton, UK) with glucose culture medium up to the concentration of about $0.5 - 3 \times 10^6$ cells. Development Buffer (DB; DictyBase recipe: 5 mM Na_2HPO_4, 5 mM KH_2PO_4, 1 mM $CaCl_2$, 2 mM $MgCl_2$; pH 6.5) was chosen as the medium for FA chemotaxis experiments because it is a well-defined medium and is an approximation of a physiological environment due to its low ionic strength [8]. A negative aspect of using DB is cell starvation and progression into development after 6+ hours (depending on cell density) and eventual loss of FA chemotactic sensitivity [9]. This was circumvented by performing the experiment before the starvation response occurs, as indicated by cell morphology – cells still had circular shapes. Since it was shown that the HL5 medium already contains about 0.12 mg/l of FA [10] ($\sim$0.3 μM), the medium was diluted by factor $\gtrsim$30,000×, lowering the background FA concentration in the medium to at most 0.01 nM. This corresponds to about 1 molecule of FA per volume size of a Dictyostelium cell ($100\,\mu m^3$). Depending on the cell concentration, 1-5 ml of cell suspension was taken from the shaken culture and DB was added for a total volume of 10 ml (dilution $\geq$2×). The cell suspension was then centrifuged for 40 seconds at 1000 RPM (200 g force), 9.8 ml of supernatant was removed, and 9.8 ml of DB was added to again have the final volume of 10 ml (dilution 50×); this was repeated once more (another dilution of 50×). 9.8 ml of supernatant was removed again and finally, 0.2 ml of 1μm diameter colloidal particles at concentration 10^8 particles/ml (Polysciences, Inc.) in DB and 1-5 ml of DB was added, depending on the starting cell concentration (dilution $\gtrsim$6×). The colloidal particles allowed us to monitor unintended convection that could ruin the static gradient. The entire procedure took about 20-30 minutes after which the cells were immediately loaded into the microfluidic device with an already established gradient.

Microfluidics device design

The microfluidic device was designed as an agarose gel containing 3 channels [11]: the static middle channel and two flowing side channels, that represent fixed boundary conditions, were separated by a layer of agarose gel and the gradient was formed by waiting for diffusion of FA to reach a steady state (see Fig.2 andFig.3). Reservoirs were connected via Teflon tubing and the steady flow was supplied by a Harvard PHD 2000 syringe pump. The time to reach the steady state was checked by running a 2D diffusion simulation in COMSOL Multiphysics 3.5 (COMSOL, www.comsol.com) and analyzing the gradient in the middle of the channel (Fig.3). The microfluidic channel containing Dictyostelium cells, also contained 1μm-sized colloidal particles. These were used to monitor the flow rate in the static channel and the measured Peclet number Lv/D (dimensionless number characterizing the ratio of advective versus diffusive transport) was always below 0.3, where L is the channel height (250 μm), D the diffusion constant of folic acid 194 μm^2/s [12] and v the measured average drift velocity of colloidal particles (0.04 to 0.23 μm/s). After loading the cells, the gradient in the middle channel was temporarily lost, however, the time-scale of diffusive refilling of that channel from the bulk of the material above is estimated to be only $t \sim L^2/D \approx 5$ minutes, an insignificant duration.

Device preparation

The 3% agarose gel was formed as follows. 0.300g of agarose was mixed with 10 ml of DB. The agarose mixture was heated and kept near the boiling point in a microwave oven for 40 seconds total. Agarose was molded by pouring the heated mixture over an inverted PDMS master, which was itself molded from an original Teflon master produced by conventional milling. After about 2 minutes the agarose solidified, the holes were punched and the chamber was secured between a plexiglas manifold and a glass microscope slide. In this experiment 3% agarose serves as an environment permeable to small molecules, such as water and folic acid, but not permeable to Dictyostelium. Dictyostelium are

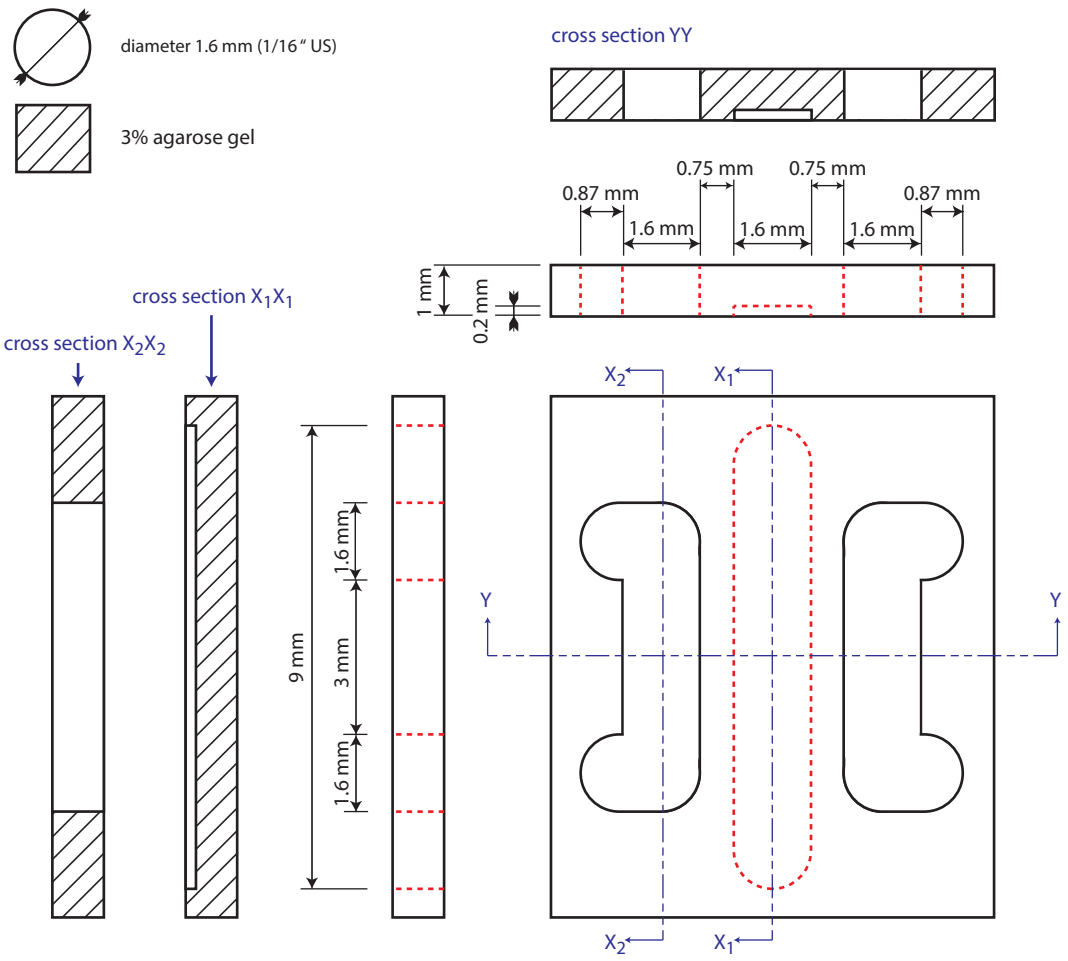

FIG. 2. A schematic of the microfluidic device used here.

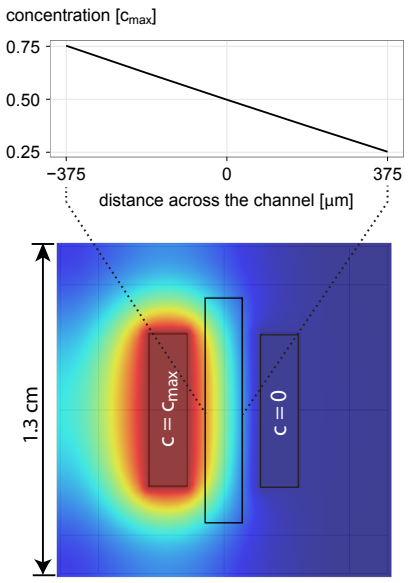

FIG. 3. Numerical 2D time-dependent simulation of diffusion through the agarose based microfluidic device used in this work, indicating a steady state gradient in the middle chamber. The top graph shows a FA concentration at the center of the channel 5 hours after the gradient started forming, in units of the FA concentration in the left channel, c_{max} (a slice through the middle of bottom figure). The bottom figure shows a concentration profile intensity of FA at the time of recording, 5 hours after the gradient started forming. Note the steady state has not been formed in the entire device, but only in the middle chamber.

migrating naturally attached on the glass surface, with 250 μm of static liquid (DB+FA gradient) on top and around them. The agarose gel was sealed well enough that the cells were unable to crawl underneath it.

Cell recording

For each run, at t=0 hours: the gradient formation was started. At t=3 hours: the cells were loaded in the device. Since we noticed that cells were not very mobile when first introduced into the device, we allowed them to adjust to the new environment for about 3.3 hours to establish a good degree of mobility. At t=6.3 hours recording started. At t=9.3 hours: the recording stopped. This time was chosen based on the fact that this is the time when one would first observe morphological changes associated with cell-to-cell cAMP signaling during the starvation response (e.g. elongated cells and formation of streams) when the cell density was significantly (10x) higher. Cell motion was recorded using bright field time-lapse optical microscopy, using an Olympus IX71 inverted microscope and a Home Science Tools MI-DC5000 5.0 Megapixel camera. Snapshots were taken every 30 seconds and cell trajectories were later analyzed on a computer. The list of concentrations used in both channels is shown in Table I.

combination	dc/dx (nM/μm)	c_0 (nM)	c_{high} (nM)	c_{low} (nM)
1	3.20×10^{1}	5.0×10^{4}	1.00×10^{5}	0
2	6.4×10^{0}	1.0×10^{4}	2.00×10^{4}	0
3	3.2×10^{0}	5.0×10^{3}	1.00×10^{4}	0
4	1.6×10^{0}	2.5×10^{3}	5.00×10^{3}	0
5	6.4×10^{-1}	1.0×10^{3}	2.00×10^{3}	0
6	3.2×10^{-1}	5.0×10^{2}	1.00×10^{3}	0
7	1.6×10^{-1}	2.5×10^{2}	5.00×10^{2}	0
8	3.2×10^{-2}	5.0×10^{1}	1.00×10^{2}	0
9	3.2×10^{-3}	5.0×10^{0}	1.00×10^{1}	0
10	3.2×10^{-4}	5.0×10^{-1}	1.00×10^{0}	0
11	0	0	0	0
12	0	2.5×10^{3}	2.50×10^{3}	2.50×10^{3}
13	0	1.0×10^{4}	1.00×10^{4}	1.00×10^{4}
14	3.2×10^{-1}	5.0×10^{3}	5.50×10^{3}	4.50×10^{3}
15	1.6×10^{0}	7.5×10^{3}	1.00×10^{4}	5.00×10^{3}
16	3.2×10^{0}	1.5×10^{4}	2.00×10^{4}	1.00×10^{4}
17	3.2×10^{0}	5.0×10^{4}	5.50×10^{4}	4.50×10^{4}
18	3.2×10^{-1}	5.0×10^{4}	5.05×10^{4}	4.95×10^{4}

TABLE I. List of experimentally used concentrations in the two channels of a microfluidic device, c_{high} and c_{low} with calculated gradient dc/dx and the mean concentration c_0.

Analysis of cell trajectories

We used ImageJ (http://imagej.nih.gov/ij/) with ParticleTracker Plugin [13] for automated cell detection and tracking. Particle tracks were analyzed in a custom-made MATLAB (The MathWorks, Natick, MA) code, where the following filtering was applied: the cells that could not be tracked consistently for more than 6 minutes (3% of the total recording time) were discarded and points on the screen that did not move at all were discarded as well; the latter corresponding to dead cells or other artifacts on the glass surface or CCD. Each experimental run was repeated 3 to 11 times, until about 300 to 700 cell trajectories were gathered. A sample of such trajectories is shown in Fig.4. The distribution of trajectories was very broad with lengths of $260 \pm 220 \mu$m. Depending on the gradient, component of the velocity in gradient direction ranges from -0.15 μm/min to 0.51 μm/min.

Analysis of different trajectory time lengths

Here we experimentally check for the possibility that cells can integrate multiple gradient measurements over time scales longer than the pseudopod extension time ($\sim$ 30 s). We calculated the chemotactic index (CI) as we progressively moved the end point of the cell trajectory from the one at frame 2 (30 seconds) to the one at frame 400 (3.3 hours).

The 30 second time interval between subsequent frames was chosen since the cell displacements were typically about 3 μm, which was at the limit for measuring displacements in our experiments.

If the cells were indeed integrating over more measurements as the time moved on, we would expect to see the CI

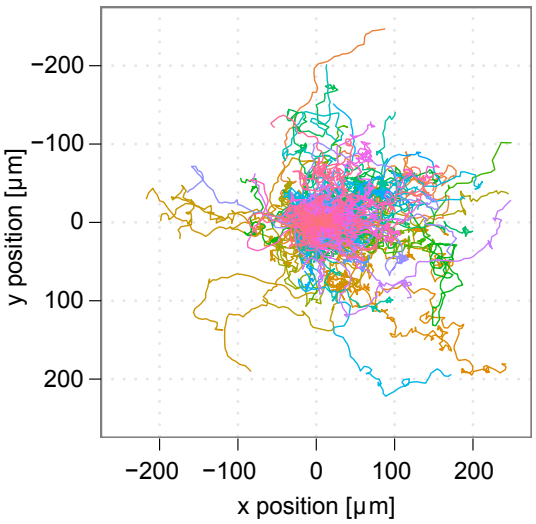

FIG. 4. Typical cell trajectories obtained from an experiment with $c_0 = 33\,K_d$ and $dc/dx = 0.11\,K_d/R$ ($K_d = 150\,\mathrm{nM}$). Different colors indicate different cell trajectories.

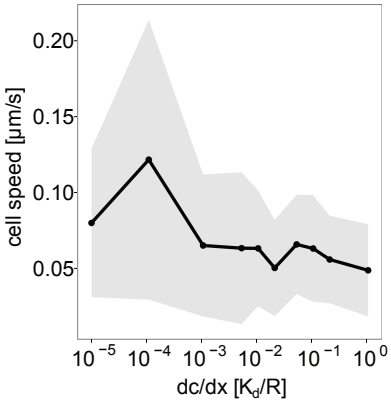

FIG. 5. Average and the standard deviation of cell speeds for the experiments given in Fig.1b in the main text. $K_d = 150\,\mathrm{nM}$, $R = 5\,\mu\mathrm{m}$.

increase with time. The results for our peak experiments with the mean concentration of 2.5 μM and the gradient of 1.6 nM/μm are shown in Fig.7. Here we see that CI actually slightly decreases after $\sim$ 300 s, but overall does not change significantly.

AVERAGING THE EXTERNAL MUTUAL INFORMATION

External mutual information I_{ext} was averaged over the entire channel in the gradient direction, weighted by the fraction of cells in each spatial segment:

$$\langle I_{ext}\rangle = \sum_{i=1}^{M} p_i I_{ext,i} \qquad (1)$$

where p_i is the fraction of cells in a segment i of the microfluidic device (a sample of such distribution is shown in

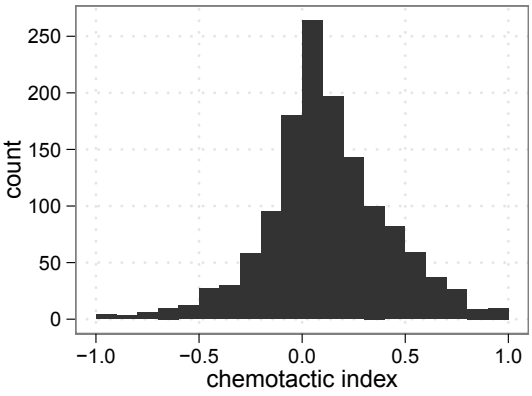

FIG. 6. Histogram showing the distribution of chemotactic index for our peak experiments with the mean concentration of 2.5 μM and the gradient of 1.6 nM/μm.

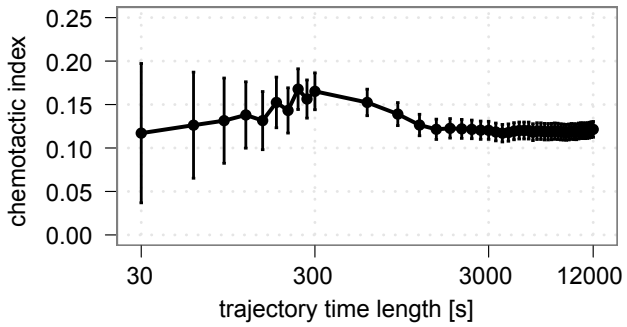

FIG. 7. Chemotactic index (CI) as a function of the trajectory time length (or the maximum allowed integration time) for a single representative experimental run with the mean concentration of 2.5 μM and the gradient of 1.6 nM/μm.

Fig.8) and $I_{ext,i} = I_{ext}(\langle c(x_i)\rangle)$ is the external mutual information for the average concentration in segment i. If I_{ext} is averaged assuming a perfectly uniform cell distribution:

$$\langle I_{ext}\rangle = \frac{1}{c_{max} - c_{min}} \int_{c_{min}}^{c_{max}} I_{ext}(c_0)dc_0 \qquad (2)$$

the analytical result is:

$$\langle I_{ext}\rangle = \frac{N}{4\ln 2\,(c_{max} - c_{min})} \times \left\{ \frac{1}{1+c_{max}} - \frac{1}{1+c_{min}} - \ln\left[\frac{(1+c_{min})c_{max}}{c_{min}(1+c_{max})}\right]\right\}$$

which agrees to our estimate of $\langle I_{ext}\rangle$ to about 10% for our experiments.

EFFECTS OF FOLIC ACID DEGRADATION

Here we explore the possibility that most of the FA is degraded by cells themselves, and they were effectively sensing a lower FA concentration, closer to K_d. FA can be degraded by an extracellular form of FA deaminase protein and we estimate the extent to which the FA concentration can be

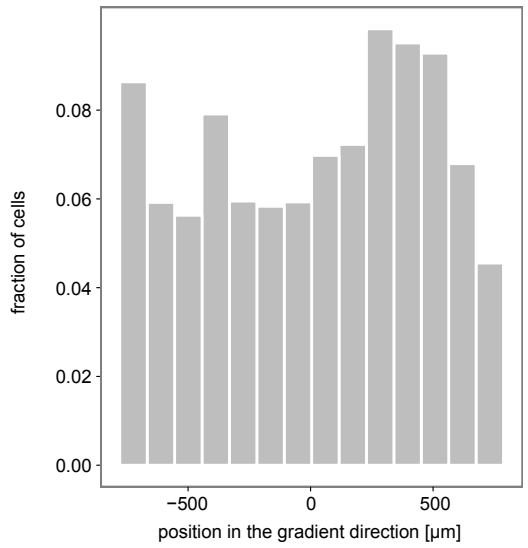

FIG. 8. The typical cell distribution as a function of the coordinate in the gradient direction, shown for the experimental run that gave the peak response with $c_0 = 2500\,\mathrm{nM}$ and $dc/dx = 1.6\,\mathrm{nM}/\mu\mathrm{m}$ for $M = 15$ segments.

reduced by this process. Following up on the previous study of the level of deaminase secretion under the same conditions [14], we estimated the deaminase activity (defined as the amount of FA degraded per cell per unit time) for our system. The reported mean value for the deaminase activity from [14] is 35 pmol per 10^6 cells per minute. Assuming a steady-state flat concentration profile of deaminase in our experiment of total volume of 0.15 ml, about 50 cells in total and about 5 hours the cells spent in the chamber (corresponding to the middle of our run), the amount of FA that could possibly be degraded by that time is 5.25×10^{-13} mol. On the other hand, the total amount of FA in this entire volume, at $2.5\,\mu$M mean concentration is 3.75×10^{-10} mol, so the degradation by FA deaminase could account for less than 0.1% of the expected amount of FA. This calculation is summarized in the Table II. This conclusion was verified experimentally by changing the cell density by a factor of four (from 7 cells/mm^2 to 30 cells/mm^2) for the gradient where we observed peak response and noticing that the same result in terms of chemotactic index (0.10 ± 0.02 at lower vs 0.09 ± 0.01 at higher density) and total mutual information (0.14 ± 0.02 bits vs 0.14 ± 0.01 bits) was observed. Thus, we conclude that degradation of FA by FA deaminase cannot account for the violation of the data processing inequality.

EFFECTS OF CELL POLARIZATION / BIAS

The total mutual information with bias is defined by:

$$I_{tot}^{bias} = H_{bias}(\theta_{res}) - H_{bias}(\theta_{res}|\theta_{grad}) \tag{3}$$

with

$$H_{bias}(\theta_{res}) = -\int p(\theta_{res};K)\log_2 p(\theta_{res};K)d\theta_{res} \tag{4}$$

quantity	value	units
activity	35×10^{-6}	pmol/(cell min)
total volume	0.15	ml
time	300	min
cell number	50	
FA amount	3.75×10^{-10}	mol
FA amount degraded	5.25×10^{-13}	mol
FA percentage degraded	0.07	%

TABLE II. Summary of the calculation for FA deaminase contribution to the observed results for the case of our best response at $2.5\,\mu$M mean concentration.

$$H_{bias}(\theta_{res}|\theta_{grad}) = -\iint p(\theta_{res}|\theta_{grad})p(\theta_{grad})\log_2 p(\theta_{res}|\theta_{grad})d\theta_{grad}d\theta_{res}$$

where the marginal probability of a response at an angle θ_{res} is:

$$p(\theta_{res};K) = \int p(\theta_{res}|\theta_{grad})p(\theta_{grad})d\theta_{grad} \tag{5}$$

which is calculated using the experimentally measured values for the distribution of the response given the gradient, $p(\theta_{res}|\theta_{grad}) = p(\theta_{res} - \theta_{grad})$. Since the measured values were discrete, we originally approximated the integral in Eq.2 (in the main text) with a discrete sum. However, here we calculated a more complicated integral and instead approximated a discrete distribution $p(\theta_{res}|\theta_{grad})$ with a continuous distribution using kernel density estimation [15]. Since this is a different method of estimating the total mutual information from the data, we first compared the results for non-biased total mutual information (corresponding to the case $K = 0$) obtained using these two methods in Fig.9 and show they are very similar. We therefore used the kernel density estimation to compute the biased total mutual information, for various values of the biasing parameter $K > 0$.

Next, we numerically calculated the biased external mutual information I_{ext}^{bias} using the Eq.13 in [16]:

$$I_{ext}^{bias} = I_{ext} - B(K) \tag{6}$$

where the term $B(K)$ depends on the bias (see [16] for details).

$$I_{ext}^{bias} = I_{ext} - \int p(\rho)h(\rho;K_p)d\rho \tag{7}$$

with:

$$I_{ext} = \frac{1}{\ln 2}\left(\frac{\nu}{\sigma}\right)^2 - \int p(\rho)\log_2 I_0\left(\frac{\rho\nu}{\sigma^2}\right)d\rho \tag{8}$$

$$p(\rho;\nu,\sigma) = \frac{\rho}{\sigma^2}\exp\left[-\frac{\rho^2+\nu^2}{2\sigma^2}\right]I_0\left[\frac{\rho\nu}{\sigma^2}\right] \tag{9}$$

$$\nu(N,c_0,\nabla c) = \frac{N}{2}\frac{\nabla c}{c_0+1} \tag{10}$$

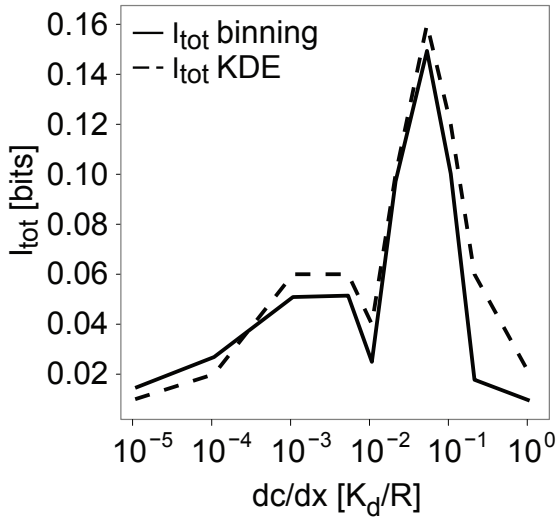

FIG. 9. Comparison of two methods for calculating I_{tot}: first binning the data and approximating the integral for I_{tot} with a sum and the second, approximating the discrete data with a continuous function obtained by kernel density estimation [15], showing that both methods give very similar results. Here we used $K_d = 150\,\mathrm{nM}$ and $R = 5\,\mu\mathrm{m}$.

$$\sigma(N, c_0) = \sqrt{\frac{N}{2}\frac{c_0}{(c_0+1)^2}} \tag{11}$$

$$h(\rho; K_p) = \frac{1}{\ln 2}\left[K\frac{I_1(K_p)}{I_0(K_p)} - \ln I_0\left(\frac{\rho\nu}{\sigma^2}\right)\right] \tag{12}$$

$$K_p = \frac{K\nu\rho}{K\sigma^2 + \nu\rho} \tag{13}$$

where c_0 is the local chemoattractant concentration in units of K_d, ∇c the gradient in units of K_d/R, N the total number of receptors, K the same biasing parameter and $I_0(K_p)$, $I_1(K_p)$ are the modified Bessel functions of the first kind of order zero and one, respectively. We computed both the total and external mutual information for different magnitudes of the bias, up to very sharp polarizations $K = 80$ (larger values require significantly higher numerical precision) and show the results in Fig.3c in the main text. These results show that the inclusion of this effect still results in the violation of the data processing inequality, and moreover, for a wide range of bias parameters, the violation is further increased.

EFFECTS OF BINNING

The total mutual information calculated using Eq.3 (main text) depends on the choice of number of bins m.

While there is no "best" number of bins, here the total number of bins chosen was 14 which gave similar results for all combinations of gradients and mean concentrations since we had roughly the same number of cells in each case (typically around 500). First, as stated in the main text, it correlates well with the CI (comparing Fig.1b and 2a in the main text). Second, I_{tot} reaches a plateau in this bin range and becomes lower when we use too few bins (below ≈ 10) or higher but with much larger uncertainty if we use too many bins (roughly 30 or more); see Fig.10. The plateau corresponds to the middle ground here where I_{tot} does not change much if the bin number changes a little around the chosen value. Finally, this choice of 14 bins gave approximately the same results as the Kernel Density Estimate (Fig.9) used for data smoothing [15].

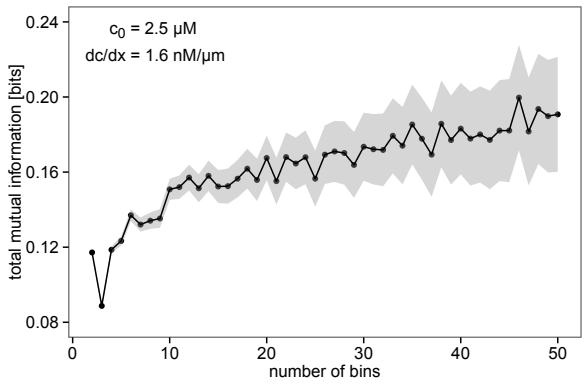

FIG. 10. The dependence of the total mutual information I_{tot} on the number of bins for the experiment with $c_0 = 2.5$ μM and $dc/dx = 1.6$ nM/μm. Shaded area shows the error in estimating I_{tot} according to the ref.[18] in the main text.

[1] S.P. Strong, R. Koberle, R.R.D. van Steveninck, W. Bialek 1998. Phys. Rev. Lett. 80:197-200
[2] T. Gregor, D.W. Tank, E.F. Weischaus, W. Bialek 2007. Cell 130:153-164
[3] C.E. Shannon 1948. Bell Syst. Tech. J. 27:379-423 and 623-656
[4] D. Fuller, W. Chen, M. Adler, A. Groisman, H. Levine, W.-J. Rappel and W.F. Loomis 2010. Proc. Natl. Acad. Sci. USA 107:9656-9659
[5] J.L. Rifkin 2001. Cell Motil. Cytoskeleton. 48:121-129
[6] B. Wurster and U. Butz 1980. Eur. J. Biochem. 109:613-618
[7] T.M. Cover and J.A. Thomas 2005. Elements of Information Theory. Wiley, New York, 2nd Ed., pp 34-35
[8] `http://dictybase.org/techniques/media/media.html#DB`, accessed 03/22/2012
[9] R.H. Kessin 2001. Dictyostelium: evolution, cell biology, and the development of multicellularity., Cambridge, Cambridge University Press
[10] J. Franke and R.H. Kessin 1977. Proc. Natl. Acad. Sci. USA. 74:2157-2161
[11] S.-Y. Cheng, S. Heilman, M. Wasserman, S. Archer, M.L. Shulerac and M. Wu 2007. Lab Chip. 7:763-769
[12] S. Kalimuthu and J. Abraham 2009. Biosens. Bioelectron. 24:3575-3580
[13] I.F. Sbalzarini and P. Koumoutsakos 2005. J. Struct. Biol. 151:182-195
[14] P.I.J. Kakebeeke, R.J.W. De Wit and T.M. Konijn 1980. J. Bacteriol. 143:307-312
[15] `http://reference.wolfram.com/mathematica/ref/SmoothKernelDistribution.html`, accessed 03/22/2012
[16] B. Hu, W. Chen, H. Levine, W.J. Rappel 2011. J. Stat. Phys. 142:1167-1186